ACS APPLIED MATERIALS & INTERFACES

www.acsami.org Research Article

Conditional Deoxyribozyme–Nanoparticle Conjugates for miRNA-Triggered Gene Regulation

Jiahui Zhang, Rong Ma, Aaron Blanchard, Jessica Petree, Hanjoong Jo,* and Khalid Salaita*

Cite This: ACS Appl. Mater. Interfaces 2020, 12, 37851–37861 Read Online

ACCESS | Metrics & More | Article Recommendations | Supporting Information

ABSTRACT: DNA–nanoparticle (NP) conjugates have been used to knockdown gene expression transiently and effectively, making them desirable tools for gene regulation therapy. Because DNA–NPs are constitutively active and are rapidly taken up by most cell types, they offer limited control in terms of tissue or cell type specificity. To take a step toward solving this issue, we incorporate toehold-mediated strand exchange, a versatile molecular programming modality, to switch the DNA–NPs from an inactive state to an active state in the presence of a specific RNA input. Because many transcripts are unique to cell subtype or disease state, this approach could one day lead to responsive nucleic acid therapeutics with enhanced specificity. As a proof of concept, we designed conditional deoxyribozyme–nanoparticles (conditional DzNPs) that knockdown tumor necrosis factor α (TNFα) mRNA upon miR-33 triggering. We demonstrate toehold-mediated strand exchange and restoration of TNFα DNAzyme activity in the presence of miR-33 trigger, with optimization of the preparation, configuration, and toehold length of conditional DzNPs. Our results indicate specific and strong ON/OFF response of conditional DzNPs to the miR-33 trigger in buffer. Furthermore, we demonstrate endogenous miR-33-triggered knockdown of TNFα mRNA in mouse macrophages, implying the potential of conditional gene regulation applications using these DzNPs.

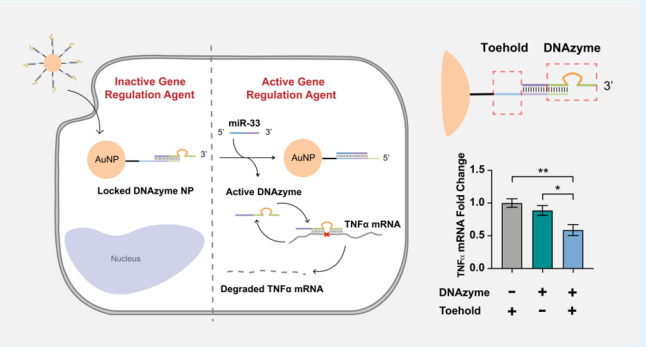

KEYWORDS: *DNA–NP conjugates, conditional gene regulation, deoxyribozyme, TNFα, miR-33, macrophages*

1. INTRODUCTION

Programmable control of gene expression is critical for constructing biological circuits for applications such as genetics research, creating models of disease, and high-specificity gene therapy. The earliest conditional gene regulation strategies include drug-inducible systems[1] and Cre-mediated excision systems,[2] which utilize regulating molecules or recombinases to trigger expression of interfering RNAs to knockdown genes of interest. Recently, conditional CRISPR-Cas9 systems utilizing structure-switchable[3] or toehold-gated guide RNA (gRNA)[4−6] have been created, which use either a ligand-induced conformational switch or toehold-mediated displacement to expose the hidden spacer region on gRNAs. Another strategy for conditional CRISPR-Cas9 systems relies on transcription of pre-gRNA flanked by miRNA binding sites, which could be processed by Dicer to release mature gRNA upon miRNA binding.[7] Despite the robustness of these systems in activating or inactivating gene expression, the need to genetically engineer the target cells or organisms using virus-based vectors and plasmid transfection for the delivery of these conditional systems hinders their potential clinical applications as gene regulatory therapeutics.

Nongenetically encoded oligonucleotides, such as siRNA, antisense, and deoxyribozymes (DNAzymes), can be transiently delivered to regulate gene expression and thus are more practical for therapeutic purposes. One prominent strategy to generate triggered oligonucleotides employs photocaging groups on the nucleotide bases to disrupt hybridization between oligonucleotides and their target mRNA.[8−10] Light irradiation uncages the oligonucleotides and thus restores their activity. Although photochemically triggered gene regulation using caged oligonucleotides provides a high degree of spatial and temporal control, this approach is limited therapeutically due to tissue damage caused by UV irradiation and the sub-mm penetration of light into tissue. In addition, this strategy relies on external intervention, thus lacking the ability to autonomously implement gene regulation based on endogenous cellular information. Therefore, conditional regulation of gene expression by oligonucleotide therapeutics in response to endogenous inputs is ideal for the purpose of smart gene regulation therapies. To achieve this goal, conditional siRNA responding to endogenous

Received: April 24, 2020
Accepted: July 28, 2020
Published: July 28, 2020

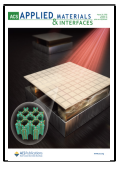

https://dx.doi.org/10.1021/acsami.0c07609
ACS Appl. Mater. Interfaces 2020, 12, 37851–37861

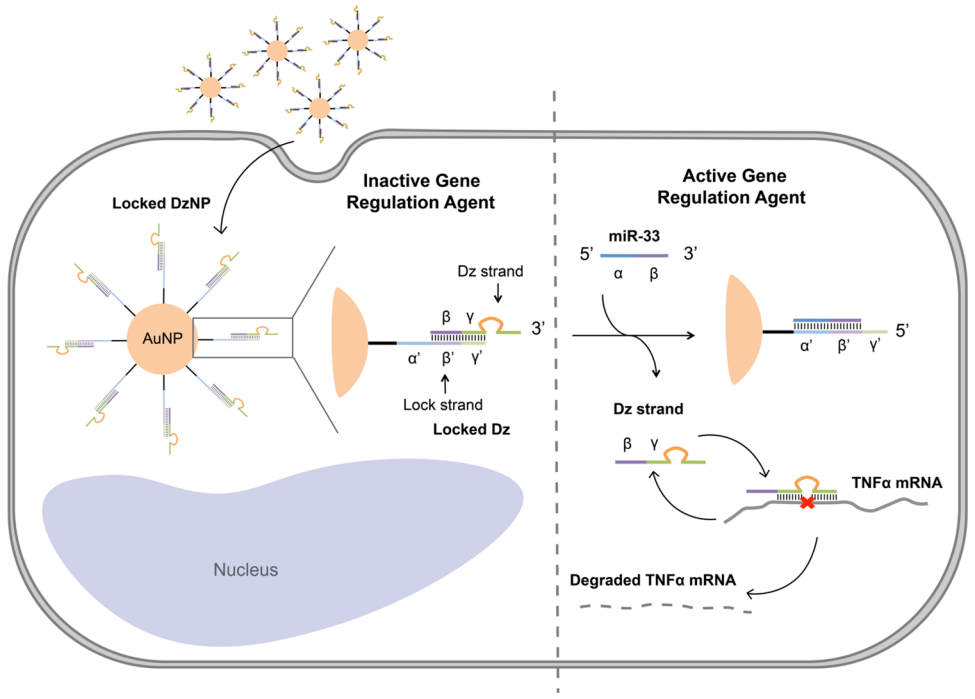

Figure 1. Schematic description of miR-33-induced TNFα knockdown by locked DzNPs. The locked DzNPs are composed of Dzs that are inactivated by hybridization to a lock strand attached to the surface of AuNPs. The lock strand consists of 3 domains: toehold domain (α'), branch migration domain (β'), and lock domain (γ'). The α' and β' domains comprise the anti-miRNA sequence, and the γ' domain is complementary to one binding arm of the DNAzyme. Since one binding arm of the Dz is blocked, its cleavage activity against its target mRNA is deactivated. However, a trigger miRNA can bind to the α' domain and initiate toehold exchange, thus leading to the release and activation of the Dz strand followed by cleavage and degradation of its target mRNA.

transcripts that drive toehold-mediated strand displacement has been created either by using a conditional Dicer substrate[11] or by the triggered assembly of siRNA.[12] These examples carry tremendous potential for toehold-gated oligonucleotides activated by endogenous nucleic acids as smart therapeutics; however, they are confronted with the common challenges facing RNA therapeutics, including stability against nucleases and poor cellular uptake.

An alternative class of gene regulatory agents is DNA−NP conjugates, or spherical nucleic acids (SNAs), which are polyvalent oligonucleotides-modified nanostructures, most commonly gold nanoparticles (AuNPs).[13] DNA−NPs confer advantages compared to linear oligonucleotides in terms of reduced susceptibility to nucleases and greater cellular uptake.[14−16] DNA−NPs have been shown to enter virtually all cell types, through a mechanism that is mediated by scavenger receptors.[17,18] Thus, DNA−NPs lack cell type or tissue specificity in their gene regulation functions. Strategies to enhance the specificity of DNA−NPs mainly involve passive targeting, which includes localized delivery by topical application[19] or enhanced permeability in tumors,[20] and active targeting via incorporating targeting moieties such as monoclonal antibodies on DNA−NPs,[21] which directs their accumulation to the targeted tissues. However, to the best of our knowledge, there are no DNA−NPs that conditionally execute gene regulation function based on the detection of intracellular inputs. Therefore, we incorporated programmability into DNA−NPs by leveraging toehold exchange, aiming to develop smart NP gene regulation agents with inherent specificity.

MicroRNAs (miRNAs) are short noncoding RNAs, which are 18−23 nucleotides (nt) in length and regulate gene expression post-transcriptionally.[22,23] They bind to the 3′-untranslated region (UTR) of target mRNAs, leading to degradation of the target mRNAs or inhibition of their translation. The specificity of miRNA for target recognition is based on Watson−Crick pairing of the 5′-seeding region (nucleotides between position 2−8 nt) of the miRNA to the complementary sequence of target mRNA. Besides their roles as key gene regulation factors, the expression levels of many miRNAs are unique in various cells and tissues under different developmental stages and pathophysiological conditions,[24,25] providing an opportunity to utilize them as a disease- or tissue-specific intracellular trigger. Here, we designed conditional DNA−NPs, in which the activity of the gene regulatory effector can be controlled by an endogenous miRNA.

The 10−23 DNAzyme is composed of a 15 nt catalytic core and two recognition arms, which can selectively bind to and degrade target mRNA.[26] Compared to siRNA therapeutics, DNAzymes offer several advantages including enhanced stability, cost-effective synthesis, and facile programmability due to their single-strand nature. Previously, we and others characterized DNAzyme−NP conjugates and showed their efficacy in regulating gene expression *in vitro*[16,27] as well as in rat models.[15] In this study, we chose miR-33 as the input and a TNFα DNAzyme as the gene regulation effector to construct a model system for miRNA-triggered gene regulation. An increased level of miR-33 is known to promote lipid accumulation in macrophages by decreasing a critical cholesterol transporter ATP-binding cassette transporter-1 (*ABCA1*) and to drive polarization of the macrophages toward the proinflammatory M1 phenotype in atherosclerosis.[28−30] During atherosclerosis development, miR-33 overexpressing lipid-laden macrophages, or foam cells, accumulate in the artery wall, where they

https://dx.doi.org/10.1021/acsami.0c07609
ACS Appl. Mater. Interfaces 2020, 12, 37851−37861

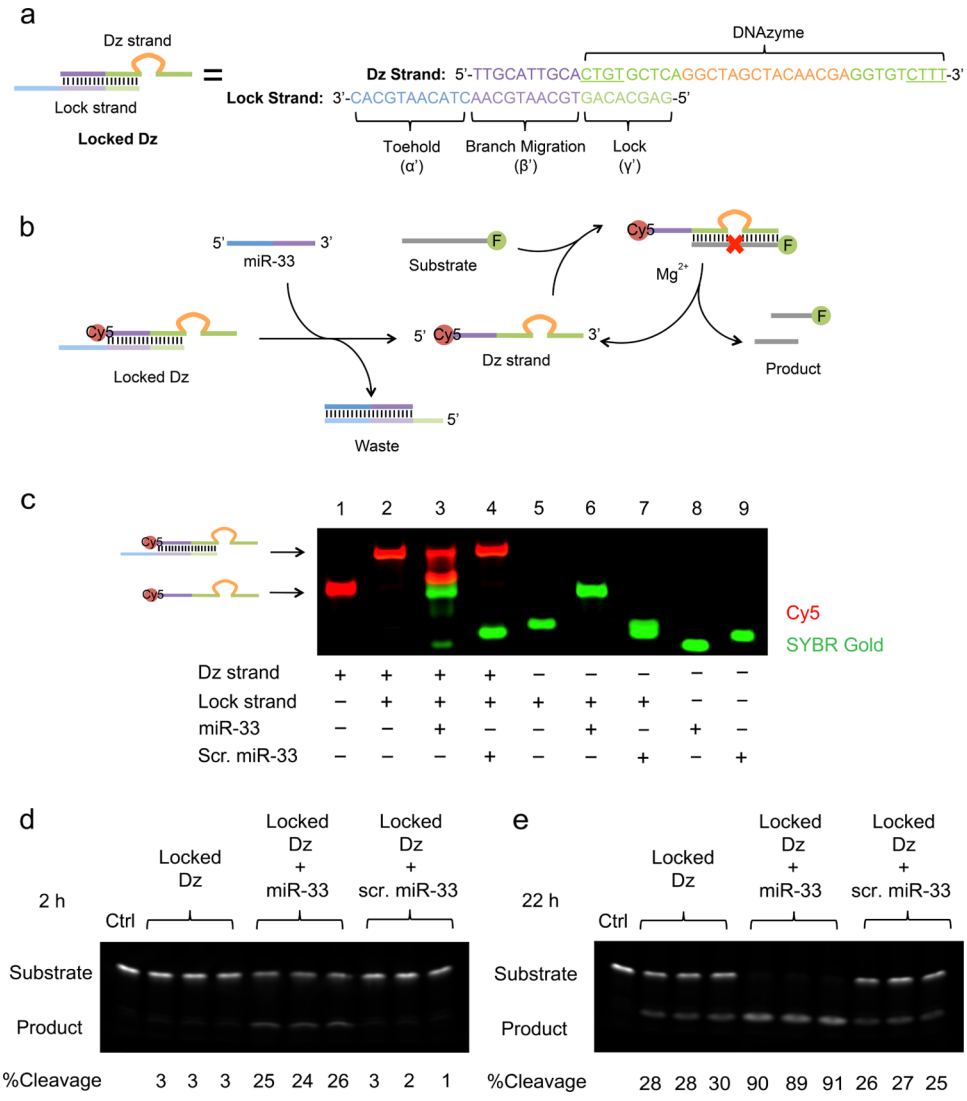

Figure 2. Design and validation of toehold exchange and activation of locked Dz by miR-33 trigger in buffer. (a) Design and sequence of locked Dz. (b) Scheme depicting activation of locked Dz by miR-33 trigger and substrate cleavage by activated Dz strand. Underscore indicates 2′-OMe modification. (c) Gel image showing toehold exchange between locked Dz and miR-33 trigger. [locked Dz] = 1 μM, [miR-33 trigger] = 1 μM, [scr. miR-33] = 1 μM, [locking strand] = 1 μM; 37 °C for 2 h. The red channel indicates Cy5 fluorescence; the green channel indicates SYBR gold staining. (d, e) Substrate cleavage activity of locked Dz incubated with miR-33 trigger or scr. miR-33. [locked Dz] = 200 nM, [miR-33 mimic] = 200 nM, [scr. miR-33] = 200 nM, [substrate] = 1 μM, [Mg^{2+}] = 2 mM; 37 °C for 2 h (d) or 22 h (e).

contribute to chronic inflammation and plaque progression by expressing proinflammatory cytokines, including TNFα.[31] Inhibition of TNFα has been shown to slow the progression of atherosclerosis,[32] but systemic inhibition of TNFα using antibody therapeutics is not problem-free as most patients develop anti-antibodies over time,[33] and it also carries an increased risk of infection and cancer as TNFα plays important roles in immune function.[34−36] The development of selective anti-TNFα therapeutics can address the limitations inherent to the systemic delivery of TNFα antibody. DNA−NP conjugates have been reported to be effectively internalized by macrophages in atherosclerotic plaques,[37] which shows their potential as therapeutic agents targeting macrophages in atherosclerosis. In addition, the cost and ease of producing DNA−NPs are significantly favorable over that of biologics. Therefore, we aimed to design conditional TNFα regulation DNA−NPs, which silence TNFα induced by a high miR-33 expression level, potentially leading to regulation of TNFα more selectively in the proinflammatory lipid-laden macrophages in atherosclerosis.

2. RESULTS AND DISCUSSION

2.1. Design of the Conditional DNAzyme NPs. Figure 1 depicts the overall design of the conditional deoxyribozyme−nanoparticles (DzNPs) and its functional mechanism. The specific sequences that we used are shown in Figure 2a. The conditional Dz is a duplex composed of a Dz strand hybridized to a lock strand, which we call the locked Dz. The lock strand consists of 3 domains: a toehold domain (α'), a branch migration domain (β'), and a lock domain (γ'). The α' and β' domains are antisense to the miRNA ($\alpha + \beta$) that serves as the trigger, and the γ' domain is complementary to the left arm (γ) of the Dz. To avoid inadvertently introducing the miR-33 seeding sequence into cells, the toehold domain (α') was designed to be complementary to the 5′ end (α) of miR-33 (Figure 2a). The Dz strand was also engineered to display the β

https://dx.doi.org/10.1021/acsami.0c07609
ACS Appl. Mater. Interfaces 2020, 12, 37851−37861

sequence of the 5′ terminus of miR-33 to stabilize binding to the lock strand. Initially, the left arm of the Dz (γ) is bound to the lock strand, inactivating its cleavage activity against the TNFα mRNA target. The locked Dzs are attached to the surface of AuNPs to form locked DzNPs to facilitate their cellular uptake. We hypothesized that, in the presence of trigger miRNA in the cytosol, the α domain of the miRNA binds to the α' domain on the lock strand and initiates toehold exchange that is driven to completion via hybridization of the miRNA's β domain to the lock strand's β' domain. This leads to unlocking of the Dz strand and thus its release from the surface of the AuNPs. The released free Dz strand is then active to cleave TNFα mRNA, leading to reduction of the TNFα levels. We ensured that the locked Dz remains hybridized at 37 °C in the absence of miR-33 by designing a thermally stable complementary sequence (*vide infra*) to minimize spontaneous activation. Note that, while the 3′ recognition (right) arm of the Dz is available for binding to TNFα mRNA as a remote toehold, such a mRNA-mediated unlocking process is hindered by the large kinetic barrier for branch migration due to the spacing introduced by the 15 nt catalytic core.[38] This is an inherent advantage to use Dzs in this design. Our results, *vide infra*, confirm this prediction. Our work also shows that only a specific miRNA can drive activation of the locked Dz because the activation barrier for dehybridization is significant and lock-miRNA toehold binding (α' to α) is essential for accelerating the unlocking process.

2.2. Screen and Optimization of Mouse TNFα DNAzyme. Based on our prior work targeting TNFα in a rat model,[15,39] we screened a small library of Dzs that target the mouse TNFα mRNA and identified a Dz that knocks down TNFα most effectively. The screen was necessary, as the prior Dz had been optimized for the rat TNFα mRNA and our present study focused on mouse models. Dz library selection was guided using a customized sequence search and binding optimization algorithm described in detail in the Supporting Information, Note 1 and Figure S1a. We selected 8 Dzs targeting different regions of mouse TNFα mRNA and transfected them in RAW264.7 cells, a mouse macrophage cell line, to evaluate their TNFα knockdown efficacy at both mRNA and protein levels (Figure S1b,c). We found that the most active Dz (Dz-168) targets the AU junction in the start codon at position 168 nt of the mouse TNFα transcript (NM_001278601.1). This Dz is similar to the prior rat/human Dz as it targets the same start codon despite having a 2 nt difference compared to the rat Dz. To maximize the Dz activity, we performed a substrate cleavage assay to compare the catalytic activity of Dzs with different binding arm lengths (7, 8, and 9 nt) as well as with or without 2′-O-Methyl (2′-OMe) modification (to enhance nuclease resistance) on the four most external nucleotides (Figure S2a,b). The Dzs were incubated with FAM-labeled substrates that mimic the mouse TNFα mRNA sequence for 140 min, and the reaction mixture was resolved using a denaturing gel (Figure S2c). We found that increasing the binding arm length from 7 to 9 nt resulted in increased Dz activity, which is likely due to enhanced binding affinity. Incorporating four 2′-OMe-modified nucleotides to the terminal ends of the binding arms led to increased activity of Dzs with 7 and 8 nt arms (from 27 to 52% and from 46 to 55% substrate cleaved, respectively), but the 9 nt arm Dz maintained a similar level of activity with and without 2′-OMe modification (65% substrate cleaved). We next compared the TNFα knockdown activity of the 2′-OMe-modified Dz with 7 and 9 nt arms in mouse primary peritoneal macrophages and found similar levels of TNFα knockdown (~60%) (Figure S2d). Based on these results, we chose to move forward with the 9 nt arm 2′-OMe-modified Dz for subsequent work, given its efficacy both in buffer and *in vitro*. Previous studies of Dz kinetics showed that designing the binding arms with too high an affinity for the substrate reduces the Dz catalytic activity by slowing the product-releasing step.[40] Therefore, aiming to further improve the Dz activity by adding more nucleotides to the binding arms or introducing modifications that enhance substrate affinity will likely have diminishing returns and may inhibit the Dz activity.

2.3. Conditional DNAzyme Activation Triggered by miR-33 in Buffer. The locked Dz was prepared by annealing the Dz strand and the lock strand at a 1:1 ratio. The Dz strand was labeled with Cy5 to facilitate visualization in gel analysis. It is important to note that the Dz modified with the β domain and Cy5 showed similar activity compared to the parental Dz lacking β domain and Cy5, based on a substrate cleavage assay as described above (Figure S3). As expected, the Dz showed a ~6-fold inhibition of activity upon locking (Figure S3). We next tested the efficiency of toehold exchange between the locked Dz and the miR-33 trigger (we used a DNA analogue of miR-33 for stability consideration) and then quantified Dz activity in buffer (Figure 2b). The locked Dz and the miR-33 trigger were incubated at 37 °C for 2 h and then analyzed by native polyacrylamide gel electrophoresis (PAGE) to determine the interactions among Dz strand, lock strand, and miR-33 trigger. A scrambled miR-33 sequence (scr. miR-33) was used as a control to verify the specificity of the toehold exchange. The gel was stained with SYBR Gold to visualize all DNA species, whereas the Cy5 fluorescence indicated the Dz strand specifically. As shown in Figure 2c, in Lane 3 loaded with locked Dz incubated with the miR-33 trigger, the Cy5 channel showed a shift in the locked Dz band, confirming its dehybridization due to toehold exchange. The percentage of unlocked Dz strands was ~61% as quantified by measuring the intensity of the bands after background subtraction. This exchange was specific as there was no shift in Lane 4 loaded with locked Dz incubated with scr. miR-33. To confirm that the miRNA rescues the Dz catalytic activity, locked Dz was incubated with miR-33 trigger along with the FAM-labeled substrates (locked Dz: miR-33: substrate = 1:1:5) at 37 °C for 2 and 22 h. Gel electrophoresis of the reaction mixtures showed that locked Dz incubated with the miR-33 trigger showed an ~8 fold increase in substrate cleavage at the 2 h time point and near completion of the substrate cleavage at the 22 h time point, whereas the locked Dz incubated with scr. miR-33 exhibited background activity (Figure 2d,e). Together, these results demonstrate the specificity of toehold exchange as well as the restoration of the Dz activity upon triggering by the miR-33-mimicking strand in buffer.

2.4. miR-33-Triggered Activation of Locked DNAzyme and TNFα Knockdown in Macrophages. To test if the endogenous miR-33 triggers activation of the locked Dz, we used RAW264.7, a mouse macrophage cell line that expresses miR-33, as a model *in vitro* system. The locked Dz was transfected into the RAW264.7 cells using Oligofectamine, and quantitative real-time polymerase chain reaction (qRT-PCR) was performed to quantify the TNFα mRNA level after 24 h incubation. Note that there is a CpG motif in the catalytic core of the DNAzyme sequence, which is known to stimulate Toll-like Receptor 9 (TLR9) signaling and induce proinflammatory cytokine expression.[41,42] To account for this background proinflammatory effect of the nucleic acid, an inactive Dz with the same catalytic core but with scrambled binding arms was used as the negative control. Unlocked Dz, or the Dz strand

https://dx.doi.org/10.1021/acsami.0c07609
ACS Appl. Mater. Interfaces 2020, 12, 37851−37861

alone, was used as the positive control. Unexpectedly, the locked Dz showed a similar level of TNFα mRNA knockdown compared to the unlocked Dz, which indicated complete activation of Dz in the RAW264.7 cells (Figure S4). We hypothesized that this result occurred due to nuclease-caused degradation of the unmodified linear DNA, specifically the α', β', and β domains, leading to unlocking in the RAW264.7 cells. To address this, we incorporated 2′-OMe modification in the α', β', β, and γ' domains. Note that the 2′-OMe modification was only introduced at the 4 nt terminus of the 3′ end of γ' domain, matching the Dz binding arm. As shown in Figure 3, the active

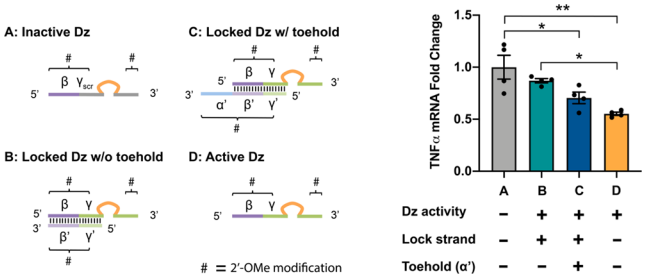

Figure 3. Endogenous miR-33-triggered activation of the locked Dz and TNFα knockdown *in vitro*. The RAW264.7 cells were transfected with 200 nM inactive Dz (A), locked Dz without the toehold (B), locked Dz with the toehold (C), or active Dz (D) with Oligofectamine and incubated for 24 h before RNA isolation and qRT-PCR quantification of TNFα mRNA. # indicates 2′-OMe modification. Dz activity: "−" indicates Dz with the scrambled binding arms, "+" indicates Dz with the TNFα mRNA complementary binding arms; Lock strand: "−" indicates that the Dz is not hybridized to a lock strand, "+" indicates that the Dz is hybridized to a lock strand; Toehold: "−" indicates the absence of the toehold, "+" indicates the presence of the toehold. The error bars represent the standard error of the mean (SEM) for the biological replicates (*$p < 0.05$, **$p < 0.01$, one-way analysis of variance (ANOVA) with Tukey's multiple comparison).

Dz strand alone knocked down TNFα mRNA by ∼45% compared to the negative control inactive Dz strand, whereas the locked Dz showed only ∼30% TNFα mRNA knockdown. To confirm that the mRNA knockdown by the locked Dz is dependent on the toehold, we also created and transfected a locked Dz with its toehold truncated, which did not show significant TNFα knockdown. These results suggest that the 2′-OMe modification helped reduce spontaneous activation caused by nucleases, and activation of the locked Dz depends on the toehold. Our attempt to further enhance TNFα knockdown with the exogenously transfected miR-33 mimics did not provide positive results (Figure S5). The RAW264.7 cells were sequentially transfected with the miR-33 mimic, then locked Dz after a 24 h interval, and allowed to incubate for another 24 h. Based on the qPCR results, the miR-33 level was increased by ∼50 fold in the miR-33 mimic-transfected cells compared to the control miRNA mimic-transfected cells (Figure S5a). Surprisingly, we observed a higher TNFα level in the miR-33 mimic-transfected cells compared to the control cells (Figure S5b). We thus hypothesized that the increased expression of TNFα was due to cross talk between miR-33 and the innate immune response, which elevates the TNFα levels. Indeed, previous literature showed that miR-33 augments TLR signaling indirectly in the macrophages by increasing cholesterol-enriched lipid raft microdomains in which the TLR complexes are assembled and activated.[43] This provides a potential explanation for why exogenously transfecting miR-33 mimic did not lead to further knockdown of TNFα by locked Dz (Figure S5).

2.5. Preparation and Characterization of Conditional DzNPs. We next sought to conjugate locked Dzs on the surface of AuNPs. Citrate-stabilized 13 nm AuNPs were prepared using published procedures.[44] AuNPs with this size were chosen because DNA−AuNP conjugates with a 13 nm AuNP core are extensively taken up by a variety of cell lines, based on our prior work[15] and studies done by Mirkin and others.[17,45] The AuNPs were monodispersed as shown by Transmission Electron Microscopy (TEM) (Figure S6a), and the AuNPs also showed an absorption peak at 520 nm (Figure S6b). At present, there are two general methods for preparation of the double-stranded DNA-conjugated NPs. The first and most commonly used method employs gradual salting of AuNPs and thiolated single-strand DNA (ssDNA) over many hours to maximize DNA packing and screen charge repulsion.[44] These NPs are then hybridized with complementary DNA. A more recent approach, which is less commonly used, utilizes freezing of thiolated ssDNA, complementary DNA, and AuNPs in a single pot.[46] Based on several screening experiments, we determined that the freezing method produced the highest density of DNA duplexes per AuNP, in agreement with the literature precedent.[46] Specifically, the Dz strand and thiolated lock strand were frozen together with AuNPs and salted to 0.3 M NaCl right before thawing at room temperature (Figure 4a).[46] The resulting

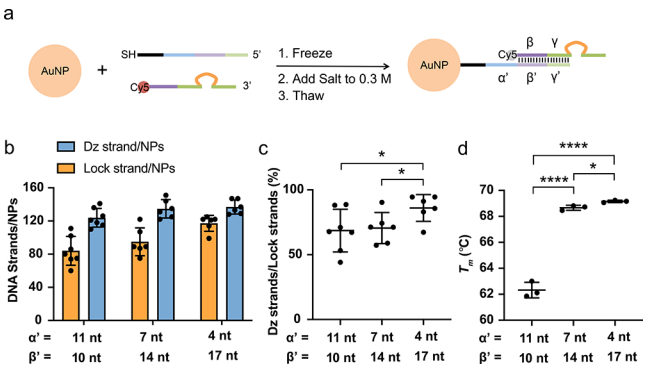

Figure 4. Preparation and characterization of the locked DzNPs. (a) Schematic showing preparation of the conditional DzNPs by freezing of the lock strand (3 μM) and Dz strand (3 μM) with AuNPs (8 nM), adding salt and thawing at room temperature. (b) Quantification of the number density of Dz strands and lock strands per AuNP. (c) Lock strand occupancy by the Dz strands as a function of the toehold (α') length. (d) T_m of the conditional DzNPs as a function of the toehold (α') length. Each data point represents an independent sample. The error bars represent the standard deviation (SD) (*$p < 0.05$, ****$p <$ 0.0001, student *t*-test).

locked DzNPs with 11 nt α' domain and 10 nt β' domain possessed an average of 84 ± 17 Dz strands per NP (Figure 4b) and a ∼69% Dz strand/lock strand ratio (Figure 4c). Furthermore, we studied the effect of the toehold length on Dz strand loading. Locked DzNPs with 7 nt toehold (α' = 7 nt, β' = 14 nt) and 4 nt toehold (α' = 4 nt, β' = 17 nt) gave an average of 95 ± 17 and 117 ± 10 Dz strands per NP and a Dz strand/lock strand ratio of 71 and 86%, respectively (Figure 4b,c). The increased loading of duplex DNA per AuNP with a reduced toehold length is likely due to the increased thermodynamic stability of the locked Dz duplex with a longer β' domain. This hypothesis is supported by the increased melting temperature (T_m) of locked DzNPs with a shorter

https://dx.doi.org/10.1021/acsami.0c07609
ACS Appl. Mater. Interfaces 2020, 12, 37851−37861

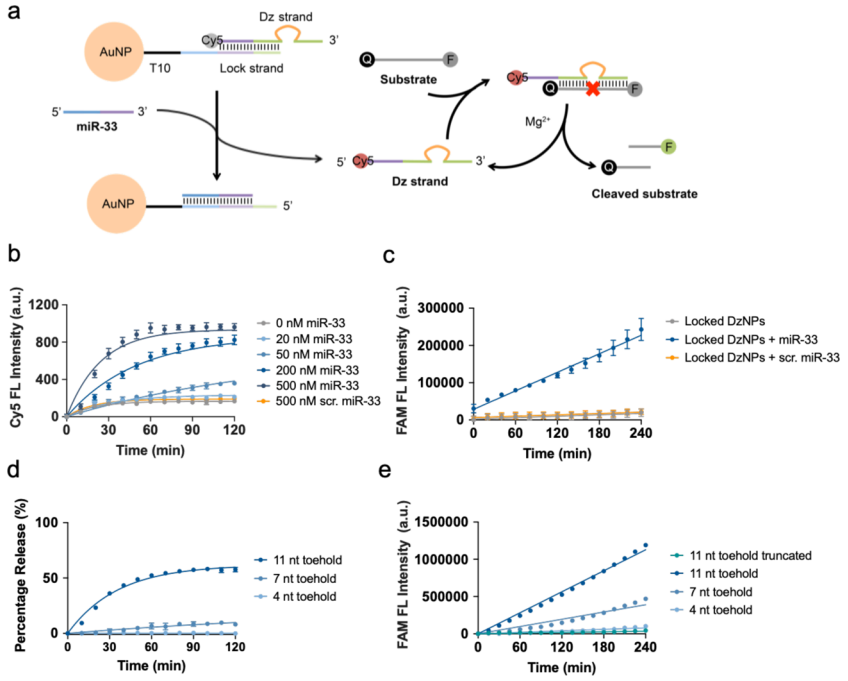

Figure 5. Activation of the locked DzNPs in buffer. (a) Scheme of the fluorogenic assay to test the release and catalytic activity of the locked DzNPs. (b) Cy5 fluorescence intensity of 0.5 nM locked DzNPs incubated with different concentrations (0, 5, 20, 50, 200, 500 nM) of the miR-33 trigger or 500 nM scr. miR-33 at 37 °C for 2 h. The error bars represent SD (n = 3). (c) 0.5 nM locked DzNPs were preincubated with 500 nM miR-33 trigger or scr. miR-33 at 37 °C. After 1 h incubation, 300 nM fluorogenic substrate was added and FAM fluorescence intensity was measured for 4 h. The error bars represent SD (n = 3). (d) Percentage release of the Dz strands from 0.5 nM AuNPs incubated with 500 nM miR-33 trigger. The error bars represent SD (n = 3 for the 11 and 7 nt toeholds, n = 1 for the 4 nt toehold). (e) 0.5 nM locked DzNPs with different toehold lengths and Dz activity were preincubated with 500 nM miR-33 trigger. After 1 h incubation, 300 nM fluorogenic substrate was added and the FAM fluorescence intensity was measured for 4 h. The error bars represent SD (n = 3) and some of them are too small to show in the plot.

toehold length: T_m of 11, 7, and 4 nt toehold-locked DzNPs were measured to be 62.3 ± 0.6, 68.7 ± 0.2, and 69.2 ± 0.1 °C, respectively (Figures 4d and S7a–c). The hydrodynamic diameters of locked DzNPs with 11, 7, and 4 nt toeholds were 72.7 ± 3.2, 82.8 ± 14.0, and 88.0 ± 4.7 nm, as measured by dynamic light scattering (DLS) based on the number distribution of their sizes (Figure S7d–g). The ζ-potentials of locked DzNPs with 11, 7, and 4 nt toehold were measured to be −14.6 ± 2.8, −16.8 ± 0.5, and −14.1 ± 1.2 mV, respectively, compared to −2.8 ± 1.6 mV for the citrate-stabilized AuNPs (Figure S7h).

The kinetics of Dz unlocking and subsequent substrate cleavage of the locked DzNPs were studied using time-resolved fluorescence assays. To quantify the Dz activity, the substrate was labeled with FAM and Black Hole Quencher (BHQ) at its termini. Upon cleavage, FAM fluorescence increases, thus reporting the catalytic activity of the Dz strand (Figure 5a). We compared the locked DzNPs of the two configurations, with either the lock strand or Dz strand directly attached to the surface of AuNPs, by tuning the position of the thiol group. The lock strand-attached locked DzNPs released Cy5-labeled Dz strands in response to the miR-33 trigger, causing an increase of Cy5 fluorescence due to separation from the AuNP and dequenching of Cy5. As miR-33 trigger concentration was increased, there was a more rapid and more complete release of the Dz strands, as indicated by the Cy5 signal (Figure 5b). This response was specific, as scr. miR-33 did not trigger the release of the Dz strands (Figure 5b). The locked DzNPs triggered with miR-33 were catalytically active and cleaved their substrates, causing an increase of FAM fluorescence, whereas the locked DzNPs alone or locked DzNPs incubated with scr. miR-33 were not able to cleave the substrates (Figure 5c). An alternative design with the Dz strand attached to the AuNPs (Figure S8a) also released the Cy5-labeled lock strands in the presence of the miR-33 trigger (Figure S8b) and the NPs were also able to cleave the substrates (Figure S8c). However, with the same concentration of the locked DzNPs (0.5 nM) and miR-33 trigger (500 nM), this design exhibited a reduction in the catalytic activity compared to the locked strand-attached DzNPs (Figure S8d), despite the higher loading of the Dz strands per NP (Dz/NPs = 126; lock strand/NPs = 97). This reduction in the catalytic activity, which is consistent with our prior work,[16] is likely due to the reduced activity of the immobilized Dz strands compared to their soluble counterparts because of a steric hindrance for substrate binding. Note that for the locked DzNPs with the immobilized Dz strands, there was a substantial amount of the Dz strands that were not hybridized with the lock strands. However, these Dz strands exhibited negligible substrate cleavage activity. A possible explanation is that the Dz strands that were not accessible for lock strand hybridization were also not accessible for substrate binding. Since the attachment of the Dz strands to the AuNPs led to a reduced Dz activity, the configuration shown in Figure 5a is preferable to the one shown in Figure S8a and was chosen for *in vitro* studies.

Interestingly, we found that the lengths of the toehold domain (α') and the branch migration (β') domain controlled the toehold exchange rate in buffer. By adjusting the lengths of the α' and β' domains, we were able to tune the release rate of the Dz strands and the cleavage rate of the substrates. 0.5 nM locked DzNPs with 11, 7, and 4 nt toehold released about 58, 10, and 0.4% Dz strands after incubation with 500 nM miR-33 trigger for 2 h (Figure 5d). The locked DzNPs with a reduced toehold

https://dx.doi.org/10.1021/acsami.0c07609
ACS Appl. Mater. Interfaces 2020, 12, 37851−37861

length showed reduced substrate cleavage activity when incubated with the same concentration of the miR-33 trigger, due to fewer released Dz strands (Figure 5e). The locked DzNPs with the toehold truncated showed a negligible substrate cleavage activity compared to the inactive DzNPs control (Figure 5e), confirming the toehold dependency of Dz activation.

2.6. miR-33-Triggered TNFα Knockdown by Locked DzNPs in the Macrophages. The cellular uptake of the locked DzNPs was assessed by fluorescence imaging of the RAW264.7 cells after 1−24 h incubation with 5 nM Cy5-labeled locked DzNPs (Figure S9a). We observed substantial internalization of NPs at the 1 h time point and further increased internalization at the 4 h time point. The time scale of uptake was consistent with the previous work.[16,47] The fluorescence intensity of the cells decreased at 16 and 24 h time points, likely due to oxidation or degradation of Cy5 over time. The internalization of the locked DzNPs was confirmed by Z-stack confocal microscopy (Figure S9b,c). We also investigated the effect of serum on the cellular uptake of the locked DzNPs. A previous study has shown that serum proteins can adsorb to DNA−AuNPs and enhance cellular uptake of G-rich DNA−AuNP but not poly-T DNA−AuNPs by THP-1 monocytes in the presence of serum.[48] Another study showed that IgG and human serum albumin adsorption lead to reduced uptake of DNA−AuNPs by the THP-1 cells.[49] In addition, it has been reported that in the presence of bovine serum albumin, the cellular binding of the anionic NPs is inhibited.[50] These studies suggest that the amount and type of the proteins adsorbing on DNA−AuNPs influence their cellular uptake differently. To study the effect of serum on our system specifically, we incubated the Cy5-labeled locked DzNPs with RAW264.7 cells for 4 h and performed flow cytometry to quantify cell-associated fluorescence. As shown in Figure S9d,e, the cells incubated with the locked DzNPs showed slightly enhanced uptake in the presence of serum.

To test miR-33-triggered TNFα knockdown *in vitro*, we designed four types of conditional DzNPs (Figure 6a) that validate the role of the toehold and the Dz activity in mediating gene regulation. Again, to account for the background proinflammatory effect caused by the CpG motif in the Dz catalytic core, the locked inactive DzNPs were used as a negative control. These NPs present an inactive Dz, which has the same 10−23 catalytic core as the active Dz, but with scrambled binding arms. This locked inactive DzNPs also contained the same toehold and branch migration domains as the locked active DzNPs. In addition, the locked DzNPs lacking the toehold domain and the locked DzNPs with a scrambled toehold domain were included as controls to further confirm the role of the toehold in triggered TNFα knockdown. These NPs were incubated with the RAW264.7 cells for 24 h before the TNFα mRNA levels were quantified with qRT-PCR. The locked DzNPs with the 11 nt toehold knocked down TNFα mRNA by ~41% compared with the locked inactive DzNP control (Figure 6b). If the 11 nt toehold of the locked DzNPs was truncated (locked DzNPs without the toehold), there was a weak (~11%) but not statistically significant TNFα knockdown. The 4-fold reduction in TNFα knockdown efficacy after removing the toehold (α') domain demonstrates that the activation of gene regulation depends on the toehold-mediated release of the Dz strands. The locked DzNPs with the scrambled toehold also showed weak, but not significant TNFα knockdown (~23%) compared to the negative control. This result may be due to a combination of nuclease-mediated unlocking of the Dz as well

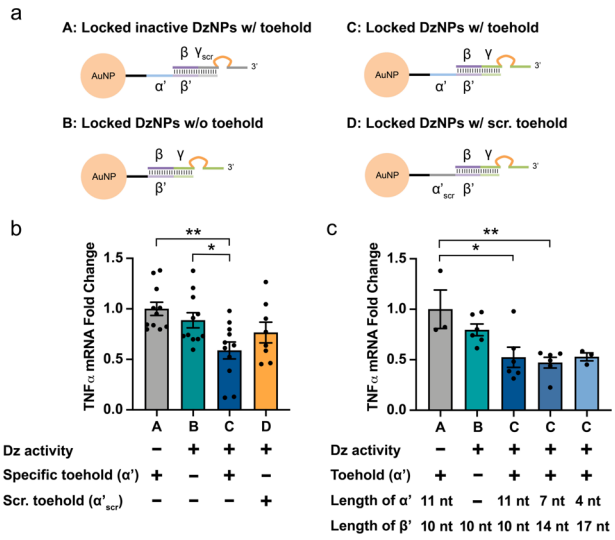

Figure 6. miR-33 triggered TNFα knockdown by the locked DzNPs *in vitro*. (a) Schematic description of the locked inactive DzNPs w/ the toehold, locked DzNPs w/o the toehold, locked DzNPs w/ the toehold, and locked DzNPs w/ the scr. toehold. (b) Effect of the toehold on TNFα knockdown. The RAW264.7 cells were incubated with the 5 nM locked inactive DzNPs w/ the toehold, locked DzNPs w/o the toehold, locked DzNPs w/ the toehold, and locked DzNPs w/ the scr. toehold for 24 h (α' = 11 nt, β' = 10 nt). TNFα mRNA was quantified by qRT-PCR. Dz activity: "−" indicates Dz with the scrambled binding arms, "+" indicates Dz with the TNFα mRNA complementary binding arms; Specific toehold: "−" indicates the absence of a miR-33 complementary toehold, "+" indicates the presence of a miR-33 complementary toehold; Scr. toehold: "−" indicates the absence of a scrambled toehold, "+" indicates the presence of a scrambled toehold. The error bars represent SEM of the biological replicates (*$p < 0.05$, **$p < 0.01$, one-way ANOVA with Tukey's multiple comparison). (c) Effect of the toehold length on TNFα knockdown. The RAW264.7 cells were incubated with 5 nM locked inactive DzNPs w/ the toehold, locked DzNPs w/o the toehold, and locked DzNPs w/ the 11, 7, and 4 nt toehold for 24 h. TNFα mRNA was quantified by qRT-PCR. The error bars represent SEM of the biological replicates (*$p < 0.05$, **$p < 0.01$, one-way ANOVA with Tukey's multiple comparison).

the binding of other endogenous transcripts to the scrambled toehold driving background activation of the Dz.

We further investigated the effect of the toehold length on TNFα knockdown efficacy. We again found that TNFα mRNA knockdown was dependent on the availability of a specific toehold and also on the catalytical active Dz (Figure 6c). In contrast to their differential activity in buffer, the locked DzNPs with shorter toehold lengths did not show the difference in the TNFα knockdown activity (Figure 6c). This finding may be due to a number of factors including the continuous expression of miR-33 in the cells, which may be different to the consumption of the miR-33 trigger in buffer. Also, the long incubation duration *in vitro* may lead to further activation of the locked DzNPs with shorter toeholds. Finally, nucleases present in the cells may also accelerate the release of the Dz strands. Regardless, these experiments clearly show that TNFα knockdown using the conditional DzNPs and this activity require a specific miR-33 complementary toehold along with the active Dz.

3. CONCLUSIONS

Conditional DzNPs are desirable smart gene regulation agents due to their molecularly specific response and their ability to be

https://dx.doi.org/10.1021/acsami.0c07609
ACS Appl. Mater. Interfaces 2020, 12, 37851−37861

transiently and easily delivered into cells rather than genetically encoded. In this study, we demonstrated a proof of concept for the conditional DzNPs that can be activated by endogenous miR-33 in macrophages. We demonstrated miR-33-triggered release and activation of the conditional DzNPs in buffer and *in vitro* and investigated the effect of configuration and toehold length on their activity. This work provides an example of intracellular toehold-mediated interaction between an endogenous transcript and "pro-drug" conditional DzNPs, which holds promise for targeted gene therapy with reduced off-target effects. Our design is modular, and thus in principle one can engineer triggered DzNPs against a wide variety of targets that are activated using different transcriptional inputs. Targeted and cell-specific delivery of drugs, including nucleic acid-based drugs, is now part of the FDA-approved arsenal of therapies to treat multiple diseases, including breast cancer (Enhertu) and acute hepatic porphyria (Givosiran). The common targeting mechanism involves conjugating antibodies or ligands to a drug molecule, thus resulting in enhanced uptake of the molecule in the cells expressing specific surface markers. We envision that the conditional DzNPs will be critical in drug targeting when a specific surface marker is absent to allow for discrimination between cell types. The vast majority of proteins are intracellular and hence mutations in cytoplasmic proteins cannot be used in conventional drug-homing mechanisms. In this case, cell type-specific or mutated transcripts are potential triggers to switch on the activity of silenced therapeutics, including conditional DzNPs, in the diseased tissues. To this end, the discovery of cell type- or disease-specific transcripts and the development of potent oligonucleotide therapeutics are indispensable. However, the precise mechanism of Dz activation of our system is unclear and it is possible for the triggering step to occur on the AuNP surface or alternatively, the triggering could occur after the locked duplex is released off the AuNP. Additionally, nuclease activity will also contribute to background activation of the Dz. Figure S10 illustrates the potential pathways of Dz activation and eventual DNA degradation. To further address the challenge of nuclease cleavage-induced spontaneous activation of conditional oligonucleotide-NP conjugates, incorporating chemical modification of oligonucleotides may further improve robust ON/OFF behavior in physiological conditions. For this purpose, the effect of chemical modifications on toehold exchange reaction kinetics needs to be investigated in greater detail. Conditional DNA−NP conjugates also have substantial applications in programmable gene regulation. Toehold-mediated strand exchange has been demonstrated as a versatile and universal molecular programming language to construct logic gates, molecular circuits, and networks. Moving forward, the conditional DNA−NP conjugates could be potentially designed to bridge multiple native transcripts and synthetic gene regulatory agents via logic gates to realize more complex functions via biocomputing.

4. EXPERIMENTAL SECTION

4.1. Materials. All oligonucleotides (Table S1), the library of DNAzymes (Table S2), and primers for qRT-PCR (Table S3) were custom-synthesized by Integrated DNA Technologies (IDT), except for the fluorogenic substrate, which was custom-synthesized by BioSearch Technologies. 15% Mini-PROTEAN TBE-Urea Gel was acquired from Bio-Rad. RNeasy Mini Kit, miScript II RT Kit, and miScript Primer Assays were acquired from QIAGEN. Quant-iT OliGreen ssDNA Assay Kit (Invitrogen), Oligofectamine Transfection Regent (Invitrogen), High-Capacity cDNA Reverse Transcription Kit (Applied Biosystems), PerfeCTa SYBR Green FastMix Reaction Mixes (QuantaBio), TNFα Mouse ELISA Kit (Invitrogen), *mir*Vana miR-33 mimic (#4464066), and *mir*Vana negative ctrl mimic (#4464058) were acquired from ThermoFisher Scientific.

4.2. Screen for Mouse TNFα DNAzyme. A library of mouse TNFα DNAzymes (Table S2) predicted with a customized algorithm were screened in RAW264.7 cells. 200 nM of each DNAzyme was transfected into RAW264.7 cells using Oligofectamine according to the manufacturer's protocol. After 24 h incubation, the cell medium was collected for ELISA analysis of secreted TNFα. QIAzol was then added into the wells to lyse the cells and total RNA was isolated using a RNeasy Mini Kit per manual. RNA was reverse-transcribed using a High-Capacity cDNA Reverse Transcription Kit. The TNFα mRNA level was quantified by qRT-PCR using PerfeCTa SYBR Green FastMix Reaction Mixes (QuantaBio) with 0.25 μM of custom-designed primers (Table S3) with Applied Biosystems StepOnePlus real-time PCR system. The relative quantification of the TNFα mRNA level was determined using the $\Delta\Delta$Ct method with 18s mRNA as a reference.

4.3. Optimization of Mouse TNFα DNAzyme in Buffer. 200 nM of DNAzymes with different arm lengths and modification were incubated with 1 μM FAM-labeled substrates in 50 mM Tris-HCl supplemented with 150 mM NaCl and 2 mM $MgCl_2$ with pH 7.4. After incubation in a water bath at 37 °C for 2 h 20 min, the reaction mixture was mixed with the same volume of gel loading buffer and subjected to 15% Mini-PROTEAN TBE-Urea Gel. The gel was run with 170 V in 1 × TBE buffer and imaged with an Amersham Typhoon Biomolecular Imager using the FITC channel. The percentage cleavage of the substrate was quantified by measuring the intensity of the substrate or product bands after background subtraction using ImageJ.

4.4. Labeling of the Dz Strands With Cy5. To label the Dz strand with Cy5 for the purpose of examination of toehold exchange, 20 μL of the 1 mM amine-modified Dz strands was mixed with 100 μg of Cy5-NHS ester dissolved in 20 μL of dimethyl sulfoxide (DMSO), 20 μL of 1M $NaHCO_3$, 20 μL of 10 × phosphate buffer saline (PBS), and 120 μL of nanopure water. The mixture was allowed to react on an orbital shaker overnight. The mixture was diluted with a 1:4 ratio with nanopure water and run through P2 gel and a Nap-25 column or high-performance liquid chromatography (HPLC) for purification.

4.5. Demonstration of Toehold Exchange and Activation of the Locked Dz in Buffer. The locked Dz was prepared by annealing the lock strand and the Cy5-labeled Dz strands at a 1:1 ratio in PBS by incubating at 95 °C for 5 min and 25 °C for 30 min in a thermocycler. The toehold exchange between the locked Dz and miR-33 trigger was examined by native PAGE gel electrophoresis. 1 μM locked Dz was incubated with 1 μM miR-33 trigger or scr. miR-33 in a water bath at 37 °C for 2 h, and then the reaction mixture was mixed with the same volume of gel loading buffer and loaded in 10% nondenaturing polyacrylamide gel. The gel was run with 110 V in cold 1 × TBE buffer and post stained with 1 × SYBR Gold for 15 min. Then, the gel was imaged using the Amersham Typhoon Biomolecular Imager with both FITC and Cy5 channels.

To demonstrate the miR-33-triggered Dz activity, 200 nM locked Dz was incubated with 200 nM miR-33 trigger or scr. miR-33 as well as 1 μM FAM-labeled substrates in a water bath at 37 °C for 2 h and then the reaction mixtures were resolved with 15% Mini-PROTEAN TBE-Urea Gel and imaged with the Amersham Typhoon Biomolecular Imager, as described above. The percentage cleavage of the substrates was quantified by measuring the intensity of the substrate or product band after background subtraction using ImageJ.

4.6. Synthesis of AuNPs. The citrate-stabilized 13 nm AuNPs were prepared using the published procedures.[44] 200 mL of 1 mM hydrogen tetrachloroaurate(III) trihydrate solution was heated to a vigorous boil in a three-neck round-bottom flask. Then, 20 mL of 38.8 mM sodium citrate tribasic dehydrate solution was added quickly, and the color of the mixture was changed swiftly from clear to purple to red. The reaction mixture was allowed to reflux for 15 min and cooled down to room temperature. The mixture was filtered through a 0.45 μm acetate filter to produce monodisperse AuNPs. The absorption peak of the AuNPs is at 520 nm determined by UV−vis spectrometry.

4.7. Preparation of Locked DzNPs. The locked DzNPs were prepared using the freezing method according to the literature.[46] 1

https://dx.doi.org/10.1021/acsami.0c07609
ACS Appl. Mater. Interfaces 2020, 12, 37851−37861

mLof 8 nM AuNPs was mixed with 3 μL of the 1 mM thiol-modified lock strand (3 nmol) and 3 μL of the 1 mM Dz strand (3 nmol) in a 1.5 mL tube. Note that the thiol-modified lock strand was used directly as acquired form IDT without reduction. The tube was frozen in a −30 °C freezer for at least 3 h. 176 μL of salting buffer (2 M NaCl in 10 mM phosphate buffer) was added into the tube right before thawing, resulting in a final NaCl concentration of 0.3 M. The mixture was allowed to thaw at room temperature. After thawing, the NPs were centrifuged down with 13 000 rpm for 20 min and washed with PBS for three times. The absorbance of NPs was measured with Nanodrop at a wavelength of 520 nm. The concentration of NPs was calculated with the following equation.

$$\text{conc.} = \frac{\text{abs}}{2.7} \times 100\ (\text{nM})$$

4.8. Quantification of the Lock Strands and Dz Strands on the Locked DzNPs. The Cy5-labeled Dz strand was used to quantify the Dz strands per NPs. A standard curve was prepared by diluting a stock of Cy5-labeled Dz strands to 0.01, 0.1, 0.2, 0.5, 0.75, and 1 μg/mL in 1 × TE buffer to a final volume of 100 μL in a 96-well plate. The locked DzNPs were diluted to 0.2, 0.4, and 0.6 nM in 1 × TE buffer to a final volume of 100 μL in the same plate. The AuNPs were then dissolved by adding 1 μL of 5 M potassium cyanide (KCN) in the wells and incubating for 30 min. Fluorescence intensity (Ex/Em = 630/670 nm) of each well was then measured using a Bio-Tek Cytation 5 Multi-Mode plate reader to determine the concentration of the Dz strands per well. The number of the Dz strands per NP was calculated by dividing the concentration of the Dz strands by AuNP concentration.

The commercial Quant-iT Oligreen ssDNA Kit was used to determine the number of lock strands per NP. The locked DzNPs were washed with nanopure water for 3 times to dehybridize the Dz strands from AuNPs, remaining only the lock strands. A standard curve was prepared by diluting a stock of the lock strand to 0.01, 0.1, 0.2, 0.5, 0.75, and 1 μg/mL to a final volume of 100 μL in 1 × TE buffer. The washed locked DzNPs were diluted to 0.2, 0.4, and 0.6 nM in 1 × TE buffer. The AuNPs were then dissolved by adding 1 μL of 5 M KCN in the wells and incubating for 30 min. 100 μL of freshly prepared 1 × Oligreen solution was added to each well and mixed by pipetting. Fluorescence intensity (Ex/Em = 485/528 nm) of each well was then immediately measured using a Bio-Tek Cytation 5 Multi-Mode plate reader to determine the concentration of the lock strands per well. The number of the lock strands per NP was calculated by dividing the concentration of the lock strands by AuNP concentration.

4.9. Hydrodynamic Size and ζ-Potential Measurement. The hydrodynamic size and size distribution of the locked DzNPs in PBS were measured by dynamic light scattering (DLS) using a Particulate System NanoPlus zeta/nano particle analyzer with a glass cuvette at room temperature. For each measurement, the hydrodynamic sizes of 100 particles were calculated, and the peak values of their number distributions were reported. ζ-Potentials of the locked DzNPs in PBS and the citrate-stabilized AuNPs in water were also measured using the same instrument at room temperature.

4.10. Release Kinetics of the Dz Strands from the Locked DzNPs and Determination of Percentage Release. 90 μL of PBS containing different concentrations of miR-33 trigger or scr. miR-33 in a 96-well plate was preincubated at 37°. 10 μL of the 5 nM locked DzNPs was added into each well (final concentration = 0.5 nM) and mixed briefly, and the fluorescence intensity (Ex/Em = 630/670 nm) was immediately measured with a Bio-Tek Cytation 5 Multi-Mode plate reader at 37 °C for 4 h with an interval of 5 min. To determine the percentage release of the Dz strands, the end point fluorescence measurement after 4 h incubation at 37 °C was conducted in a separate experiment to avoid inaccuracy caused by photobleaching in kinetic measurements. Fluorescence intensity of T10 NPs with the matched quantity of the Cy5-labeled Dz strands calculated with the Dz strands/NPs as determined above was used as a standard to mimic 100% release.

4.11. miR-33-Triggered Activation of the Locked DzNPs. 500 nM of miR-33 trigger or scr. miR-33 trigger and 0.5 nM conditional DzNPs were mixed in 97 μL of 35 mM Tris-HCl buffer (pH = 7.4) containing 150 mM NaCl and 2 mM $MgCl_2$. The mixture was preincubated at 37 °C for 1 h to allow activation of the Dz strands. 3 μL of 10 μM fluorogenic substrate was then added to each well and mixed briefly. The fluorescence intensity (Ex/Em = 485/528 nm) of each well was measured immediately with a Bio-Tek Cytation 5 Multi-Mode plate reader at 37 °C for 4 h with an interval of 5 min.

4.12. Cell Culture. RAW264.7 mouse macrophages were maintained in Dulbecco's modified Eagle's medium (DMEM) with 4.5 mg/L glucose, containing 10% (v/v) fetal bovine serum (FBS), penicillin (100 U/mL), and streptomycin (100 mg/mL), 1500 mg/L sodium bicarbonate, 1 mM sodium pyruvate, and 2 mM L-Glutamine at 37 °C under a humidified atmosphere of 5% CO_2. The RAW264.7 cells with the passage number between 10 and 13 were used in the entire study. The mouse peritoneal macrophages were isolated from the mouse peritoneal cavity according to the published procedure.[51] Briefly, 10 mL of cold medium (RPMI supplement with 10% FBS, 100 U/mL penicillin, and 100 mg/mL streptomycin) was injected into the abdominal cavity of the mouse and the fluid is slowly removed with a syringe after carefully shaking the mouse for 5 min. The cells were spun down by centrifugation at 15 000 rpm for 8 min at 4 °C. The cell pellet was resuspended in the medium and plated in a 12-well plate. The unattached cells were washed away with PBS after 4 h and the adhered cells were incubated overnight for the treatment the following day.

4.13. Fluorescence Imaging and Confocal Imaging to Assess Cellular Uptake. The RAW264.7 cells were seeded in 8-well chambers on a glass slide with 5×10^4 cells per well. 5 nM of the 11 nt toehold locked DzNPs (with the Cy5-labeled Dz strands) was incubated with the RAW264.7 cells for 1 to 24 h in complete medium. After washing with PBS to remove the NPs that were unbound and not internalized, the cells were imaged immediately at 150× magnification with the Cy5 channel on a Nikon Eclipse Ti2 microscope.

To confirm internalization of the locked DzNPs inside the cells, RAW264.7 cells were incubated with 5 nM 11 nt toehold locked DzNPs (with the Cy5-labeled Dz strands) for 4 h and washed with FluoroBrite DMEM medium once to remove the unbound and not internalized NPs. FluoroBrite DMEM medium was then added to the wells. The Z-stack confocal images were taken with a step size of 0.2 μm on a Nikon Ti Eclipse inverted confocal microscope with a Plan Apo Lambda 60×/1.40 Oil objective.

4.14. Flow Cytometry to Investigate the Effect of Serum on Cellular Uptake. RAW264.7 cells were seeded in a 12-well plate with a density of 2×10^5 cells per well the day before the experiment. 5 nM Cy5-labeled locked DzNPs were added to the cells in the presence or absence of serum. After 4 h, the cells were washed with cold Hank's Balanced Salt Solution (HBSS) for 3 times, and the cells were removed from the surface using cell scrapers. The cells were pelleted by centrifugation and resuspended in HBSS for flow cytometry measurement of cell-associated fluorescence.

4.15. *In Vitro* Knockdown of TNFα With Locked Dzs or Locked DzNPs. For testing the locked Dz, RAW264.7 cells were seeded in a 48-well plate with a density of 5×10^4 cells per well the day before transfection. 200 nM of inactive Dz, locked Dz with the toehold, locked Dz without the toehold, and active Dz were transfected into the cells using Oligofectamine according to the manufacturer's protocol. The cells were incubated for 24 h, and RNA was isolated for quantification of TNFα mRNA using qRT-PCR as described above.

For testing the locked DzNPs, RAW264.7 cells were seeded in a 48-well plate with a density of 5×10^4 cells per well the day before treatment. 5 nM of locked inactive DzNPs, locked DzNPs with the toehold (different toehold lengths), locked DzNPs without the toehold, and locked DzNPs with the scrambled toehold were incubated with RAW264.7 cells for 24 h in complete medium, and RNA was isolated for quantification of TNFα mRNA using qRT-PCR as described above.

4.16. qRT-PCR of miR-33. The cells were lysed with QIAzol reagent and total RNA was isolated with miRNeasy Mini Kit (QIAGEN) following the manufacturer's protocol. RNA was reverse-transcribed using miScript II RT Kit (QIAGEN). qPCR of miR-33 was conducted using miScript Primer Assays (QIAGEN) with PerfeCTa SYBR Green FastMix Reaction Mixes (QuantaBio). The relative quantification of the miR-33 level was determined using the ΔΔCt method with RNU6 as a reference.

https://dx.doi.org/10.1021/acsami.0c07609
ACS Appl. Mater. Interfaces 2020, 12, 37851−37861

4.17. Statistics. All statistical analyses were performed using Graphpad Prism software. The quantitative results of TNFα knockdown *in vitro* were presented as mean ± SEM. Statistical analyses were performed by one-way analysis of variance (ANOVA) followed by the post-test multiple comparison as described in the figure captions. *P* values of less than 0.05 were considered significant.

■ ASSOCIATED CONTENT

Supporting Information

The Supporting Information is available free of charge at https://pubs.acs.org/doi/10.1021/acsami.0c07609.

Additional supporting experiments, including screen and optimization of mouse TNFα DNAzyme, activation of the Dz strand-attached locked DzNPs, cellular uptake of the locked DzNPs, and all oligonucleotide sequences (PDF)

Software 1: customized algorithm for DNAzyme prediction (ZIP)

Spreadsheet 1: predicted TNFα DNAzymes by customized algorithm (XLSX)

■ AUTHOR INFORMATION

Corresponding Authors

Hanjoong Jo − *Wallace H. Coulter Department of Biomedical Engineering, Georgia Institute of Technology and Emory University, Atlanta, Georgia 30332, United States; Division of Cardiology, Department of Medicine, Emory University, Atlanta, Georgia 30322, United States*; Email: hjo@emory.edu

Khalid Salaita − *Wallace H. Coulter Department of Biomedical Engineering, Georgia Institute of Technology and Emory University, Atlanta, Georgia 30332, United States; Department of Chemistry, Emory University, Atlanta, Georgia 30322, United States*; orcid.org/0000-0003-4138-3477; Email: k.salaita@emory.edu

Authors

Jiahui Zhang − *Wallace H. Coulter Department of Biomedical Engineering, Georgia Institute of Technology and Emory University, Atlanta, Georgia 30332, United States*; orcid.org/0000-0002-4949-6217

Rong Ma − *Department of Chemistry, Emory University, Atlanta, Georgia 30322, United States*

Aaron Blanchard − *Wallace H. Coulter Department of Biomedical Engineering, Georgia Institute of Technology and Emory University, Atlanta, Georgia 30332, United States*

Jessica Petree − *Department of Chemistry, Emory University, Atlanta, Georgia 30322, United States*

Complete contact information is available at: https://pubs.acs.org/10.1021/acsami.0c07609

Funding

This work was supported in part by funding from the National Institutes of Health grants R01HL142866 to K.S. and RHL119798 and HL095070 to H.J. H.J. is also supported by the Wallace H. Coulter Distinguished Professor Chair fund.

Notes

The authors declare no competing financial interest.

■ ACKNOWLEDGMENTS

We would like to thank Michael Davis Lab at Emory University for providing the RAW267.4 cells.

■ REFERENCES

(1) Szulc, J.; Wiznerowicz, M.; Sauvain, M.-O.; Trono, D.; Aebischer, P. A Versatile Tool for Conditional Gene Expression and Knockdown. *Nat. Methods* **2006**, *3*, 109−116.

(2) Tiscornia, G.; Tergaonkar, V.; Galimi, F.; Verma, I. M. Cre Recombinase-Inducible RNA Interference Mediated by Lentiviral Vectors. *Proc. Natl. Acad. Sci. U.S.A.* **2004**, *101*, 7347−7351.

(3) Liu, Y.; Zhan, Y.; Chen, Z.; He, A.; Li, J.; Wu, H.; Liu, L.; Zhuang, C.; Lin, J.; Guo, X.; et al. Directing Cellular Information Flow Via CRISPR Signal Conductors. *Nat. Methods* **2016**, *13*, 938−994.

(4) Siu, K.-H.; Chen, W. Riboregulated Toehold-Gated Grna for Programmable CRISPR−Cas9 Function. *Nat. Chem. Biol.* **2019**, *15*, 217−220.

(5) Jin, M.; Garreau de Loubresse, N.; Kim, Y.; Kim, J.; Yin, P. Programmable CRISPR-Cas Repression, Activation, and Computation with Sequence-Independent Targets and Triggers. *ACS Synth. Biol.* **2019**, *8*, 1583−1589.

(6) Hanewich-Hollatz, M. H.; Chen, Z.; Hochrein, L. M.; Huang, J.; Pierce, N. A. Conditional Guide Rnas: Programmable Conditional Regulation of CRISPR/Cas Function in Bacterial and Mammalian Cells Via Dynamic RNA Nanotechnology. *ACS Cent. Sci.* **2019**, *5*, 1241−1249.

(7) Wang, X.-W.; Hu, L.-F.; Hao, J.; Liao, L.-Q.; Chiu, Y.-T.; Shi, M.; Wang, Y. A MicroRNA-Inducible CRISPR−Cas9 Platform Serves as a MicroRNA Sensor and Cell-Type-Specific Genome Regulation Tool. *Nat. Cell Biol.* **2019**, *21*, 522−530.

(8) Young, D. D.; Lively, M. O.; Deiters, A. Activation and Deactivation of Dnazyme and Antisense Function with Light for the Photochemical Regulation of Gene Expression in Mammalian Cells. *J. Am. Chem. Soc.* **2010**, *132*, 6183−6193.

(9) Young, D. D.; Lusic, H.; Lively, M. O.; Yoder, J. A.; Deiters, A. Gene Silencing in Mammalian Cells with Light-Activated Antisense Agents. *ChemBioChem* **2008**, *9*, 2937−2940.

(10) Hemphill, J.; Liu, Q.; Uprety, R.; Samanta, S.; Tsang, M.; Juliano, R. L.; Deiters, A. Conditional Control of Alternative Splicing through Light-Triggered Splice-Switching Oligonucleotides. *J. Am. Chem. Soc.* **2015**, *137*, 3656−3662.

(11) Hochrein, L. M.; Schwarzkopf, M.; Shahgholi, M.; Yin, P.; Pierce, N. A. Conditional Dicer Substrate Formation Via Shape and Sequence Transduction with Small Conditional RNAs. *J. Am. Chem. Soc.* **2013**, *135*, 17322−17330.

(12) Ren, K.; Zhang, Y.; Zhang, X.; Liu, Y.; Yang, M.; Ju, H. In Situ Sirna Assembly in Living Cells for Gene Therapy with MicroRNA Triggered Cascade Reactions Templated by Nucleic Acids. *ACS Nano* **2018**, *12*, 10797−10806.

(13) Cutler, J. I.; Auyeung, E.; Mirkin, C. A. Spherical Nucleic Acids. *J. Am. Chem. Soc.* **2012**, *134*, 1376−1391.

(14) Giljohann, D. A.; Seferos, D. S.; Prigodich, A. E.; Patel, P. C.; Mirkin, C. A. Gene Regulation with Polyvalent siRNA-Nanoparticle Conjugates. *J. Am. Chem. Soc.* **2009**, *131*, 2072−2073.

(15) Somasuntharam, I.; Yehl, K.; Carroll, S. L.; Maxwell, J. T.; Martinez, M. D.; Che, P.-L.; Brown, M. E.; Salaita, K.; Davis, M. E. Knockdown of TNF-$\alpha$by DNAzyme Gold Nanoparticles as an Anti-Inflammatory Therapy for Myocardial Infarction. *Biomaterials* **2016**, *83*, 12−22.

(16) Yehl, K.; Joshi, J. P.; Greene, B. L.; Dyer, R. B.; Nahta, R.; Salaita, K. Catalytic Deoxyribozyme-Modified Nanoparticles for RNAi-Independent Gene Regulation. *ACS Nano* **2012**, *6*, 9150−9157.

(17) Choi, C. H. J.; Hao, L.; Narayan, S. P.; Auyeung, E.; Mirkin, C. A. Mechanism for the Endocytosis of Spherical Nucleic Acid Nanoparticle Conjugates. *Proc. Natl. Acad. Sci. U.S.A.* **2013**, *110*, 7625−7630.

(18) Patel, P. C.; Giljohann, D. A.; Daniel, W. L.; Zheng, D.; Prigodich, A. E.; Mirkin, C. A. Scavenger Receptors Mediate Cellular Uptake of Polyvalent Oligonucleotide-Functionalized Gold Nanoparticles. *Bioconjugate Chem.* **2010**, *21*, 2250−2256.

(19) Zheng, D.; Giljohann, D. A.; Chen, D. L.; Massich, M. D.; Wang, X.-Q.; Iordanov, H.; Mirkin, C. A.; Paller, A. S. Topical Delivery of siRNA-Based Spherical Nucleic Acid Nanoparticle Conjugates for Gene Regulation. *Proc. Natl. Acad. Sci. U.S.A.* **2012**, *109*, 11975−11980.

(20) Jensen, S. A.; Day, E. S.; Ko, C. H.; Hurley, L. A.; Luciano, J. P.; Kouri, F. M.; Merkel, T. J.; Luthi, A. J.; Patel, P. C.; Cutler, J. I.; et al. Spherical Nucleic Acid Nanoparticle Conjugates as an RNAi-Based Therapy for Glioblastoma. *Sci. Transl. Med.* **2013**, *5*, 209ra152.
(21) Zhang, K.; Hao, L.; Hurst, S. J.; Mirkin, C. A. Antibody-Linked Spherical Nucleic Acids for Cellular Targeting. *J. Am. Chem. Soc.* **2012**, *134*, 16488−16491.
(22) Kumar, S.; Kim, C. W.; Simmons, R. D.; Jo, H. Role of Flow-Sensitive MicroRNAs in Endothelial Dysfunction and Atherosclerosis: Mechanosensitive Athero-MiRs. *Arterioscler., Thromb., Vasc. Biol.* **2014**, *34*, 2206−2216.
(23) Kumar, S.; Boon, R. A.; Maegdefessel, L.; Dimmeler, S.; Jo, H. Role of Noncoding RNAs in the Pathogenesis of Abdominal Aortic Aneurysm: Possible Therapeutic Targets? *Circ. Res.* **2019**, *124*, 619−630.
(24) Landgraf, P.; Rusu, M.; Sheridan, R.; Sewer, A.; Iovino, N.; Aravin, A.; Pfeffer, S.; Rice, A.; Kamphorst, A. O.; Landthaler, M.; et al. A Mammalian MicroRNA Expression Atlas Based on Small RNA Library Sequencing. *Cell* **2007**, *129*, 1401−1414.
(25) Lagos-Quintana, M.; Rauhut, R.; Yalcin, A.; Meyer, J.; Lendeckel, W.; Tuschl, T. Identification of Tissue-Specific MicroRNAs from Mouse. *Curr. Biol.* **2002**, *12*, 735−739.
(26) Santoro, S. W.; Joyce, G. F. A General Purpose Rna-Cleaving DNA Enzyme. *Proc. Natl. Acad. Sci. U.S.A.* **1997**, *94*, 4262−4266.
(27) Hartmann, A. K.; Cairns-Gibson, D. F.; Santiana, J. J.; Tolentino, M. Q.; Barber, H. M.; Rouge, J. L. Enzymatically Ligated DNA-Surfactants: Unmasking Hydrophobically Modified DNA for Intracellular Gene Regulation. *ChemBioChem* **2018**, *19*, 1734−1739.
(28) Ouimet, M.; Ediriweera, H.; Afonso, M. S.; Ramkhelawon, B.; Singaravelu, R.; Liao, X.; Bandler, R. C.; Rahman, K.; Fisher, E. A.; Rayner, K. J.; et al. MicroRNA-33 Regulates Macrophage Autophagy in Atherosclerosis. *Arterioscler., Thromb., Vasc. Biol.* **2017**, *37*, 1058−1067.
(29) Rayner, K. J.; Suárez, Y.; Dávalos, A.; Parathath, S.; Fitzgerald, M. L.; Tamehiro, N.; Fisher, E. A.; Moore, K. J.; Fernández-Hernando, C. Mir-33 Contributes to the Regulation of Cholesterol Homeostasis. *Science* **2010**, *328*, 1570−1573.
(30) Ouimet, M.; Ediriweera, H. N.; Gundra, U. M.; Sheedy, F. J.; Ramkhelawon, B.; Hutchison, S. B.; Rinehold, K.; van Solingen, C.; Fullerton, M. D.; Cecchini, K.; et al. MicroRNA-33−Dependent Regulation of Macrophage Metabolism Directs Immune Cell Polarization in Atherosclerosis. *J. Clin. Invest.* **2015**, *125*, 4334−4348.
(31) Moore, K. J.; Sheedy, F. J.; Fisher, E. A. Macrophages in Atherosclerosis: A Dynamic Balance. *Nat. Rev. Immunol.* **2013**, *13*, 709−721.
(32) Branen, L.; Hovgaard, L.; Nitulescu, M.; Bengtsson, E.; Nilsson, J.; Jovinge, S. Inhibition of Tumor Necrosis Factor-A Reduces Atherosclerosis in Apolipoprotein E Knockout Mice. *Arterioscler., Thromb., Vasc. Biol.* **2004**, *24*, 2137−2142.
(33) Bartelds, G. M.; Krieckaert, C. L.; Nurmohamed, M. T.; van Schouwenburg, P. A.; Lems, W. F.; Twisk, J. W.; Dijkmans, B. A.; Aarden, L.; Wolbink, G. J. Development of Antidrug Antibodies against Adalimumab and Association with Disease Activity and Treatment Failure During Long-Term Follow-Up. *JAMA* **2011**, *305*, 1460−1468.
(34) Scheinfeld, N. A Comprehensive Review and Evaluation of the Side Effects of the Tumor Necrosis Factor Alpha Blockers Etanercept, Infliximab and Adalimumab. *J. Dermatol. Treat.* **2004**, *15*, 280−294.
(35) Bongartz, T.; Sutton, A. J.; Sweeting, M. J.; Buchan, I.; Matteson, E. L.; Montori, V. Anti-Tnf Antibody Therapy in Rheumatoid Arthritis and the Risk of Serious Infections and Malignancies: Systematic Review and Meta-Analysis of Rare Harmful Effects in Randomized Controlled Trials. *JAMA* **2006**, *295*, 2275−2285.
(36) Mariette, X.; Matucci-Cerinic, M.; Pavelka, K.; Taylor, P.; van Vollenhoven, R.; Heatley, R.; Walsh, C.; Lawson, R.; Reynolds, A.; Emery, P. Malignancies Associated with Tumour Necrosis Factor Inhibitors in Registries and Prospective Observational Studies: A Systematic Review and Meta-Analysis. *Ann. Rheum. Dis.* **2011**, *70*, 1895−1904.
(37) Zhang, L.; Tian, X. Y.; Chan, C. K.; Bai, Q.; Cheng, C. K.; Chen, F. M.; Cheung, M. S.; Yin, B.; Yang, H.; Yung, W.-Y.; et al. Promoting the Delivery of Nanoparticles to Atherosclerotic Plaques by DNA Coating. *ACS Appl. Mater. Interfaces* **2019**, *11*, 13888−13904.
(38) Genot, A. J.; Zhang, D. Y.; Bath, J.; Turberfield, A. J. Remote Toehold: A Mechanism for Flexible Control of DNA Hybridization Kinetics. *J. Am. Chem. Soc.* **2011**, *133*, 2177−2182.
(39) Iversen, P. O.; Nicolaysen, G.; Sioud, M. DNA Enzyme Targeting TNF-α mRNA Improves Hemodynamic Performance in Rats with Postinfarction Heart Failure. *Am. J. Physiol.: Heart Circ. Physiol.* **2001**, *281*, H2211−H2217.
(40) Schubert, S.; GuÈl, D. C.; Grunert, H. P.; Zeichhardt, H.; Erdmann, V. A.; Kurreck, J. RNA Cleaving '10-23' DNAzymes with Enhanced Stability and Activity. *Nucleic Acids Res.* **2003**, *31*, 5982−5992.
(41) Lin, A. Y.; Almeida, J. P. M.; Bear, A.; Liu, N.; Luo, L.; Foster, A. E.; Drezek, R. A. Gold Nanoparticle Delivery of Modified CpG Stimulates Macrophages and Inhibits Tumor Growth for Enhanced Immunotherapy. *PLoS One* **2013**, *8*, No. e63550.
(42) Sester, D. P.; Brion, K.; Trieu, A.; Goodridge, H. S.; Roberts, T. L.; Dunn, J.; Hume, D. A.; Stacey, K. J.; Sweet, M. J. CpgGDNA Activates Survival in Murine Macrophages through TLR9 and the Phosphatidylinositol 3-Kinase-Akt Pathway. *J. Immunol.* **2006**, *177*, 4473−4480.
(43) Lai, L.; Azzam, K. M.; Lin, W.-C.; Rai, P.; Lowe, J. M.; Gabor, K. A.; Madenspacher, J. H.; Aloor, J. J.; Parks, J. S.; Näär, A. M.; Fessler, M. B. MicroRNA-33 Regulates the Innate Immune Response Via ATP Binding Cassette Transporter-Mediated Remodeling of Membrane Microdomains. *J. Biol. Chem.* **2016**, *291*, 19651−19660.
(44) Hill, H. D.; Mirkin, C. A. The Bio-Barcode Assay for the Detection of Protein and Nucleic Acid Targets Using DTT-Induced Ligand Exchange. *Nat. Protoc.* **2006**, *1*, 324−336.
(45) Deng, R.; Shen, N.; Yang, Y.; Yu, H.; Xu, S.; Yang, Y.-W.; Liu, S.; Meguellati, K.; Yan, F. Targeting Epigenetic Pathway with Gold Nanoparticles for Acute Myeloid Leukemia Therapy. *Biomaterials* **2018**, *167*, 80−90.
(46) Liu, B.; Liu, J. Freezing Directed Construction of Bio/Nano Interfaces: Reagentless Conjugation, Denser Spherical Nucleic Acids, and Better Nanoflares. *J. Am. Chem. Soc.* **2017**, *139*, 9471−9474.
(47) Wu, X. A.; Choi, C. H. J.; Zhang, C.; Hao, L.; Mirkin, C. A. Intracellular Fate of Spherical Nucleic Acid Nanoparticle Conjugates. *J. Am. Chem. Soc.* **2014**, *136*, 7726−7733.
(48) Chinen, A. B.; Guan, C. M.; Ko, C. H.; Mirkin, C. A. The Impact of Protein Corona Formation on the Macrophage Cellular Uptake and Biodistribution of Spherical Nucleic Acids. *Small* **2017**, *13*, No. 1603847.
(49) Zhang, W.; Meckes, B.; Mirkin, C. A. Spherical Nucleic Acids with Tailored and Active Protein Coronae. *ACS Cent. Sci.* **2019**, *5*, 1983−1990.
(50) Fleischer, C. C.; Payne, C. K. Nanoparticle−Cell Interactions: Molecular Structure of the Protein Corona and Cellular Outcomes. *Acc. Chem. Res.* **2014**, *47*, 2651−2659.
(51) Zhang, X.; Goncalves, R.; Mosser, D. M. The Isolation and Characterization of Murine Macrophages. *Curr. Protoc. Immunol.* **2008**, *83*, 14.1.1−14.1.14.

https://dx.doi.org/10.1021/acsami.0c07609
ACS Appl. Mater. Interfaces 2020, 12, 37851−37861